

FEDSM-ICNMM2010-3\$' - +

FLOW-STRUCTURE INTERACTION PROBLEM OF A PITCHED BASEBALL WITHOUT SPIN (KNUCKLEBALL)

Hiroshi Higuchi

Dept. of Mechanical and Aerospace Engineering
Syracuse University, Syracuse, NY

Toshiro Kiura

Institute of Fluid Science
Tohoku University, Sendai, Japan

ABSTRACT

The “knuckleball” effect is believed to be caused by asymmetric flow separation over the baseball, but little is known about its flow physics. The baseball is gripped with the knuckles in a certain position and is pitched in a way that introduces nearly no rotation, resulting in erratic flight paths which confuse batters. In the experiment described in this paper, the flow near the seams of the baseball is visualized thoroughly and the velocity vector fields near the surface and in the wake are obtained with Digital Particle Image Velocimetry. Depending on its position, the seam is found to trigger the boundary layer transition thus delaying the separation, or to cause separation itself. Three-dimensional wake patterns associated with specific ball orientations are identified and related to the force variations on the ball.

INTRODUCTION

The dynamic behavior of a sports ball has a close relationship with the fluid-structure interaction problem. Some sports balls have peculiar surface patterns, e.g. seams and/or dimples. Also these balls change their orientation during the flight, often causing irregular flight paths¹. Especially in baseball which is covered by two strips of hide tightly stitched together in a three-dimensional manner², aerodynamic forces act on the pitched ball in various directions that depend on the flight velocity, rotational speed, rotation axis and surface seams^{3,4}. The seam height is typically less than 1mm out of 72mm diameter baseball. Spinning curveballs known as ‘curve’ and ‘shoot’, have more than 30 rps of rotational speed. The ball experiences a lateral force under the

Magnus effect⁵. A ‘straight’ ball with a backspin receives a force opposite to gravity. In this sense, a straight ball may be as a type of curveball. In the case of non-spinning curveballs, such as the ‘knuckleball’, the rotational speed is approximately zero; one high-speed camera measurement reported it to be 0.28rps, resulting in only 1/4 rotation through its entire flight⁶. At this rotational speed, the boundary layer on the surface is affected by the seams, and the wake generated over the baseball is deflected by the asymmetric boundary layer separation. Some aerodynamic measurements have been reported in the past⁶⁻⁸, as well as numerical simulation of the flow⁹. However, the flow physics of the knuckleball, and in particular the boundary layer and separated flow characteristics, have not been documented. Misconceptions persist about the differences between flow behind such axisymmetric or three-dimensional bluff bodies and that behind two-dimensional counterparts³. Thus, the aim for this experiment is to analyze the relationship between the aerodynamic force and flow field generated over the baseball. Particular attention is paid to the boundary layer transition, separation and deflected wake influenced by the seams on the surface of the ball.

EXPERIMENTAL SETUP

Wind Tunnel Setup and Aerodynamic Force Measurement

The experiment was conducted with a commercially available baseball placed in an open jet of a low-speed, low-turbulence recirculating wind tunnel at the Institute of Fluid Science, Tohoku University. The nozzle was octagonal and 0.293m wide, and the distance to the diffuser entrance was 0.53m. The free stream turbulence was less than 0.2%¹⁰. The ratio between the model cross-sectional area and the upstream nozzle opening was 5%. Tests in a larger, proportionally scaled wind

*Corresponding author hhiguchi@syr.edu
+Currently at Honda R&D Co. Ltd, Japan

tunnel with a 0.81m wide nozzle¹¹ were also conducted, but the small wind tunnel of the same design was utilized because of its easier access without exhibiting any drawback due to its smaller jet. First, in order to analyze the relationship between seam position and aerodynamic force, drag and side forces are measured at each ball orientation. The experimental apparatus and coordinate system are shown in Fig. 1(a), and reference orientations of ball axes are shown in Fig. 1(b). In light of the 3-dimensionality of boundary layer separation, three different axes of baseball are chosen for study. The ball orientation about each axis is set by the stepping motor at a 0.36 degree increment. The ball is fixed stationary at each orientation until the measurement is completed. Ball axis A coincides with the y-axis, and is called the 4-seam position. A typical knuckleball is thrown in this orientation, and thus closer attention is paid to it in this paper. Ball axis B corresponds to the z-axis, which is called 2-seam. Force measurements are conducted in the range between 16m/s and 30 m/s. For most of the experiment on the flow field, however, free stream velocity is fixed at 22 m/s (79.2 km/h), which is known to be in the range of typical knuckleball velocity. The corresponding Reynolds number based on the free stream velocity and the ball diameter of 71.5 mm is 1.05×10^5 . The coordinate system with its origin at the center of the ball is chosen as shown. The ball orientation is specified in the clockwise direction as observed from above. Drag and side forces are measured with the load cell after calibrated against dead weights, and are considered positive in positive x- and z-directions. The ball was supported from below by a thin rod away from the measurement plane. In order to avoid the effect of any support on a sphere and a blunt-edged circular cylinder, some new experiments have been carried out using a magnetic support and balance system^{12,13}, but deployment of such system was not possible on an actual baseball. Comparing the drag measurements on the sphere with the present system and those with the magnetic suspension system, the effect on the present measurement was deemed insignificant for the present discussion.

Flow Visualization

Instantaneous wake pattern and flow separation at each angle and axis orientation are first visualized using paraffin smoke from a heated wire and captured with a digital CCD camera illuminated by a synchronized Nd:YAG laser sheet. In order to observe the time-dependent wake structure and the separation movement, the flow field over the baseball is illuminated by a continuous argon laser and recorded on a high-speed video camera at up to 9,000 frames per second. The smoke wire is located 2mm downstream from the end of the ball and parallel to the z-axis (see Figure 1), and multiple smoke wires are used as needed. Further flow visualizations near the surface are conducted with a uniform seeding which is used for the instantaneous

velocity vector measurement as discussed below.

Measurement of Velocity Vector Fields

The velocity vector profiles near the surface and in the wake cross sections are measured with the TSI Digital Particle Image Velocimetry (PIV) system for each angle and axis. This setup is the same as in Fig. 1, except for the uniform seeding and different arrangements for the pulsed laser light sheet and camera as needed. Smoke wires are removed and the entire test section is filled with oil mist, with particles averaging 1 micron in diameter, introduced in the downstream diffuser section.

RESULTS

Force Measurement

The relationship between time-averaged drag and side force coefficients and the ball seam angle at each of the three orientations are presented. The ball is positioned at one orientation, and data are sampled at 10 KHz and are time-averaged over 12.3 seconds and ensemble-averaged over three full rotations. The forces are normalized by the free stream dynamic pressure and the ball cross-sectional area. Uncertainty of the data is estimated to be ± 0.02 considering the precision error, repeatability and high frequency fluctuations. Flow velocity is 22 m/s, with a Reynolds number of 1.05×10^5 .

The results of the force variations at different orientations about the axis A, often called the 4-seam position, are shown in Fig. 2. As the illustration on top of the figure shows, the seam orientation of the baseball repeats itself with a 180 degrees interval, though in the meridian cross sectional plane, it exhibits a pseudo periodicity every 90 degrees. The drag coefficient varies periodically between 0.4 and 0.6 at 90 degree intervals. The minimum is at 0 degree of ball angle, while the maximum value is measured at 45 degrees. The side force experiences a much wider range of periodic variation. Measurement at the present Reynolds number shows large side force fluctuations at 90°, 180°, etc. where the time-averaged RMS level reached 0.2. Small peaks in the side force in the range between 45degrees and 58 degrees and at subsequent equivalent orientations are also noticeable.

For axes B (commonly called the 2-seam position) and C (the oblique position), the results are shown in Figs. 3 and 4, respectively. The aerodynamic force about the ball axis C showed the most gradual variation with angle, with a periodicity of 180 degrees, and that about the ball axis B showed a moderate level of variations. As comparison among Figs. 2, 3 and 4 shows, the ball orientation corresponding to the ball axis A produced the most dramatic side force variation, and the flow in this orientation was most sensitive to the change in the ball angle. Therefore, the emphasis of the experiment was placed on the ball axis A and its results are discussed further in detail.

In order to assess the force variations when the speed is

changed, force measurements are carried out for the ball axis A between 16 m/s and 30 m/s. The Reynolds number range is between 7.6×10^4 and 1.43×10^5 . The results are shown in Fig. 5. In general, similar periodic drag and side force variations with the period of 90 degrees are observed. Above 24m/s, both drag and side forces vary by smaller amount. The drag force variations are small at the lowest speed but increase with the speed up to 24 m/s. At two lowest speeds, the drag coefficient follows a slightly different pattern and does not decrease at 0 or 180 degrees unlike those at 90 and 270 degrees. The drag force average over the entire rotation decreases monotonically from 0.6 to 0.5 with speed. The Reynolds numbers in these cases are sub-critical for a smooth sphere. The side force is zero at 0° , 90° , 180° , etc. as expected within the accuracy of the ball manufacturing, alignment and force measurement. The region of extreme side force ($> \pm 0.3$) decreases with speed, and the small peaks in the side force in the range between 45 degrees and 58 degrees becomes less prominent at higher speed, whereas more prominent regions of reduced drag and slightly convoluted side force excursions are seen near 90° , 180° , etc. at higher Reynolds numbers. The force excursions in these regions will be addressed in the discussion.

In order to elucidate the cause of these variations in drag and side forces, detailed flow visualizations and velocity measurements were conducted as described below.

Wake: Flow Visualization and PIV Measurement

Flow visualization photographs with smoke wire and PIV velocity profiles using seeded particles for the x-z plane ($y=0$) are shown in Fig. 6. Coordinates are normalized by the ball diameter, d . The velocity profiles (e-h) correspond to the areas marked in the photos (a-e). The velocity vectors are ensemble-averaged from 40 instantaneous profiles. While this paper is concerned with global flow characteristics as shown, the uncertainty of the time-averaged velocity data is estimated to be less than $\pm 2\%$, deemed adequate in the present study. The free stream direction is from left to right. Change in wake size can be seen between 0° (Figs.6a, e) and 45° (Figs. 6c, g). The larger wake in the latter produces a higher drag coefficient as seen in Fig. 2, though both wakes in this cross sectional plane are symmetric and produce nearly zero side force. On the other hand, a clear sidewise flow deflection is observed in Figs. 6(b)&(f), resulting in a large side force. In Figs. 6(d)&(h), the wake is deflected in the opposite direction. At 45degrees the flow separations appear to be triggered by the seam, but this is not necessarily the case for other angles. The boundary layer behavior and its separation are addressed in the next section.

The three-dimensional wake structure is further clarified in the end view, i.e., in a cross section normal to the flow. The figures on top in Fig. 7 are smoke visualizations at $x/d=1.125$. At 0 degree (Fig. 7a), the region of the wake field is symmetric and narrow,

corresponding to a smaller drag and zero side force. At 30 degrees (Fig. 7b), the wake is deflected due to an asymmetrical boundary layer separation. As shown in the next section, close-up measurements indicate that the seam works as a tripping wire and the separation is delayed on one side of the ball. The PIV measurements were performed on the same cross sections by uniformly seeding the flow. The results in the bottom figures (Fig. 7) indicate clear vortical structure within the wake corresponding to the region indicated above. In particular, at 30 degrees (b), a pair of strong counter-rotating vortices and an induced velocity field, somewhat resembling wing-tip vortices, can be seen on the port side of the PIV result. The induced velocity and the wake deflection are consistent with the large side force observed (in this figure the force on the ball is to the right). At 0° , two pairs of counter-rotating vortices are shown resulting in a nearly balanced side force. (Note: the end view of the ball at this position will appear as in Fig. 3 at 270° .) The asymmetry is weak at 45° (c), whereas at 60° (not shown) the counter-rotating vortices are in the opposite direction of those at 30° .

Boundary Layer Behavior: Visualization and Velocity Field

In order to further clarify the relationship between the flow separation and the surface condition, the flow immediately adjacent to the ball surface was investigated. The seeded flow near the surface is shown in Figs. 8(a,b,c) for 3 different ball orientations, 30° , 45° and 60° , respectively. Separating shear layers are identifiable as dark regions which result from dearth of particles within the initial boundary layer. The variation of the separation point was small based on the high-speed video of the smoke flow visualization within its resolution, and these instantaneous photos are deemed representative of a sequence of photos captured. In Fig. 8a (30°), the separated shear layer is out of view and further downstream. The seam (typically 1mm high) appears to have triggered a boundary layer transition to turbulence thus delaying the separation in this Reynolds number range. Corresponding velocity measurements will be discussed below. Mizota et al.⁷ carried out hot wire measurements near the baseball surface at free stream velocity of 21.5m/s. They found that at 35° orientation, there was a turbulent boundary layer separation at the 110 degrees on the top surface and laminar separation at 94 degrees at the opposite side of the baseball. Incidentally they also found a turbulent boundary layer separation at 0° ball orientation around 120 degrees from the stagnation point. In Fig. 8b (45°), the boundary layer separation is caused by the seam itself. A shear-layer instability and roll-up are seen in the photo. On the other hand, the boundary layer in Fig. 8c (60°) separates over the smooth surface ahead of the seam. The seam does not play any role, because it is located in the separated, reverse flow region.

These phenomena are further analyzed quantitatively

by applying the DPIV technique. Figures 9 show the ensemble averaged velocity vector fields near the ball surfaces; detailed velocity profiles within the boundary layer and in the reverse flow regions are shown. The position of the seam is also identified in the figures. These results are obtained in the same setting as visualized in Figs. 8. At 30 degrees as shown in Fig. 9(a), the separation is substantially delayed with the seam at the shoulder position. Separation point is downstream of this viewing area ($x/d > 0.3$, $> 127^\circ$). The boundary layer is deemed turbulent as in the case of a tripped boundary layer over a sphere, and the velocity profile approaching the separation appears somewhat fuller than the counterpart in Fig. 6(d). though the PIV resolution did not allow examination of the velocity profile against the law of the wall, etc. The separation caused by the seam protrusion and a large reverse flow region are shown in Fig. 9b (45°). The separation at the seam occurs at $x/d = -0.025$ or 87° from the stagnation point. In Fig. 9c (60°), however, the separation moves ahead of the seam on the smooth surface near 84.3 degrees from the front stagnation point. The separation point is similar to that of a laminar boundary layer over a smooth surface. While the spatial resolution is limited, the separating boundary layer profile shows that the flow is laminar, in contrast to that for 30° . Figure 9d, measured at 90° , shows a flow pattern somewhat similar to that at 0° , but the boundary layer separation is slightly delayed to about 106° from the front stagnation point. Note between the 0° and 90° ball orientations, the seam location in this cross section is similar, but the three-dimensional seam configurations are different between the two. Together with the visualizations at intermediate angles, the boundary layer behavior is discussed more in detail in the next section. Recently, a numerical simulation to compute the behavior of the flow over a baseball has shown the three-dimensional nature of boundary layer separation⁸, but the flow transition and/or flow separation at specific ball orientations as identified in this paper are not demonstrated.

DISCUSSION OF FORCE VARIATION AND THE FLOW FIELD

The relationship between the force variation and the flow field has been clearly shown in the present research.

As the results in Fig. 5 have indicated, large side force variations were observed within the range of Reynolds number between 76,000 and 143,000. Similar periodic side force variations were measured by Watts and Sawyer⁸ at approximate Reynolds number of 102,000. The force variations were much smaller, about ± 0.1 in force coefficient and partly due to large stepping angle, they did not resolve sharp side force variations observed at present. They did not provide technical information on wind tunnel size or its conditions. While agreeing in

general with their measurements, the present results (see Figs. 2-5) show much more convoluted force variations in these ball orientations associated with subtle change in flow physics, and will be further addressed below again focusing on the orientation around axis A (4 seam position.).

As the ball is rotated clockwise from the symmetric seam orientation at 0° with zero side force, the seam on the upper surface trips the boundary layer and delays separation, hence the positive side force. The boundary layer is still attached at 30° in the viewing area of Fig. 8a and Fig. 9b. However, Figs. 10a and b indicate a sudden change of the boundary layer behavior when the ball orientation moved from 36° by just one degree to 37° , where the separation occurs at the seam. A closer look at Fig. 10a indicates a small separation bubble behind the seam. Within this range, the seam appears to change its role as a boundary layer trip to the cause of the boundary layer separation. Whereas the protrusion, roughness effect, and subsequent modification to the surface pressure gradient are suspected (see e.g., Schubauer and Spanngenberg¹⁶), it is beyond the scope of the current observation using the actual, non-instrumented baseball. More detailed PIV measurements or a specially made model with pressure ports may have enabled calculation of surface pressure distribution to elucidate the boundary layer behavior (see, e.g., Amitay et. al.¹⁷ for modified pressure distribution estimated from the PIV results). Elucidating the flow around the actual baseball, rather than a scale model, was the thrust of this study.

At 45° (see Fig. 8b and Fig. 9c) the seams on both sides are symmetrical and produce nearly symmetrical separated flow and wake (Figs. 6, 7) and zero side force (Fig. 2). When the ball is further rotated clockwise about the axis A, the separation caused by the seam moves with it till approximately 50° as shown in Fig. 10c. The separation takes place from the smooth surface on the opposite side of the ball resulting in large positive side force. Further rotation of the ball causes the separation to jump ahead of the seam and the side force shifts toward negative. Figure 10d taken at 52° indicates that the separation line has moved just ahead of the seam. The separation point remains the same between 52° and 80° . Though not included for brevity, the flow visualizations show that the boundary layer is again attached and the separation moved downstream of the view starting around the ball orientation 82° . Transition of the boundary layer appears to be limited in this region where the front seam is in the boundary layer development region and yet the rear seam is sufficiently downstream and out of the way. The overall minimum drag occurs when the boundary layer behavior is near symmetric on top and bottom (See Fig. 5 and Fig. 6).

It has been noted that the side force variations in the range 45° - 60° and its equivalent positions are somewhat discontinuous (see Figs. 2 and 5) and the boundary layer separation is extremely sensitive to a small change in the ball angle, and is subject to a hysteresis effect. This

point is further addressed below.

The present experiment has been conducted in a quasi-steady manner. These measurements are taken over a long sampling period while the ball is held at a position and is stepped in 0.36 degree increment to another position in one direction. The flow field remains the same with time and is not subject to change due to minor external disturbance. However, when the measurements are repeated by stepping through ball orientation in the opposite direction, the hysteresis effect has been noted, for example between 45 and 52 degrees. At 45°, flow separations caused by the top seam and the bottom seam of the ball flow field produce near zero side force. Again refer to the seam orientation in the Fig. 2. When the ball is rotated clockwise, the flow separation from the top seam moves downstream and that from the bottom seam moves upstream, causing a positive side force. The flow separations subsequently jump to the smooth surface (upstream on the top and downstream at the bottom). As this may not occur simultaneously, non-monotonic side force variations are experienced. When the ball is stepped in counterclockwise direction while the separation is ahead of the seam at 52°, the separation remains ahead of the seam until rotated down to 30°. The side force is slightly negative during this period. Near 60°, the separation from the bottom surface causes a similar hysteresis effect. The flow pattern is again relatively robust and rarely changed either with time or with upstream disruptions.

The ball axis A presented above (i.e., 4-seam position) exhibited the most force excursions per ball rotation, and this appears to be the preferred hold for knuckleball pitchers. In other ball orientations, seam pattern (see Fig. 1) modified the boundary layer through a similar mechanism, though less dramatically. It is noted that the phenomena depicted on different cross sectional planes occur simultaneously due to the non-axisymmetric seam pattern, and that the boundary layer and the wake flow field are fully three-dimensional even in the time-averaged sense. Note that side force variations shown in Figs. 2-4 at various orientations about three axes can occur simultaneously and manifest themselves as complex three-dimensional vertical and horizontal forces.

While we have focused our attention to the side force variation that affect the ball trajectory most, it is worth revisiting the drag force. Variation in drag force and that in the wake size are well correlated as reported widely for spheres and sports balls. For example, Jeon et al.¹⁴ recently applied active separation control on a smooth sphere to modify its drag. (Note, however, when the separation line is fixed as on a disk placed normal to the flow, a smaller wake produces a higher drag¹⁵.) Sawada, et al¹² used the magnetic suspension and balance system to measure the drag variation of a smooth sphere up to the critical Reynolds number. They observed a beginning of the drag decrease at Reynolds number just below 300,000. The free stream turbulence was between

0.05% and 0.07%. It may be noted that the average drag coefficient is higher than that for a smooth sphere (see e.g., Achenbach¹⁸) though the same experimental set up had been used by another group to yield nominal results for a smooth sphere. Mizota et al's drag measurements⁶ on the non-spinning baseball range between 0.4 and 0.7 with similar angle dependence as observed presently. When they varied the Reynolds number at the ball position of 35 degrees as in the present ball axis A, the drag coefficient remained higher than 0.5 for $Re=100,000 \sim 200,000$. The surface roughness would reduce the drag on smooth spheres (see, e.g., Achenbach¹⁹), but no drop in the drag was observed in this Reynolds number range. Though the baseball surface away from the seam is not completely smooth, we may conclude that the present results reflect the effect of the seam on the boundary layer and its separation. Here the fully three-dimensional seam pattern may give a clue on the phenomena observed. As shown in Fig. 1b, the seam pattern for the ball axis is highly asymmetric viewed from the side. For example the side view seam pattern at ball orientation of 0 degree for the ball axis A corresponds to the ball orientation of 90degrees of the ball axis B (compare Figs. 1b, 2 and 3). Thus the some part of the seam may work as a trip wire, the other portion of the seam triggers a three-dimensional flow separation. Further study of three-dimensional boundary layer separation and reverse flow region is needed.

High-speed video was taken of global wake oscillation in this cross sectional plane. The visualized downstream wake oscillation had a frequency equivalent to the Strouhal number of 0.21, similar to that found behind a smooth sphere.²⁰ In the high-speed video of the flow past the ball, movement of the separated shear layer angle was noted but its synchronization with the wake oscillation was not clear. In addition the movement of the separation point was not discernible (refer to Fig. 6). It is worth pointing out that the large asymmetric wake oscillation is produced also behind a sharp-edged disk with a fixed separation line (see, e.g., Bigger, et. al.¹⁵). When the power spectra of the side force were analyzed, a spectral peak was not found at that frequency. Thus the low frequency wake oscillation was deemed a non-contributing factor for the knuckleball fluctuations.

The role of the seam on the boundary layer separation and on the resulting side force has been demonstrated. In order to illuminate the mechanism of forced mixing by the seam more clearly, however, additional detailed flow-field measurements including velocity fluctuations within the boundary layer and in the immediate vicinity of the seam would be needed, but perhaps is beyond the scope of the present study using the commercially available real baseball.

In general, the knuckleball is pitched with a minimal rotation to trigger the physical behavior investigated above and to induce a combination of side force and to a lesser extent, drag force variations during its flight. The

narrow speed range needed to effect the large variation of the boundary layer behavior also makes pitching such a ball challenging. It is to be noted that even if the ball is thrown at zero rotation, the ball will still undergo slow rotation in flight due to the asymmetric surface shear stress, as also pointed out in a short comment by Weaver²¹. However, it would be a complex task to measure or numerically predict the three dimensional shear stress distribution to forecast the actual rotation. Together with the hysteresis effect discussed above, the trajectory becomes seemingly erratic and extremely difficult to determine, thus confusing the batter. While the present study identified the mechanism of the knuckleball phenomena, further study is needed before one may be able to predict the dynamic variation of ball orientation and the flow field a priori.

CONCLUSION

Detailed velocity vector field measurements and visualization study of flow over a baseball were conducted to examine the physics of the knuckleball. Large side force excursions were obtained depending on the ball orientations. The drag and side force variations were shown to be caused by the change in the size and symmetry of the recirculation region in the wake. In particular, large-scale counter-rotating vortices were shown corresponding to large side force measured. Depending on the ball orientation, the seam was found to trigger flow separation or boundary layer transition. The present study demonstrated that the pitch called the knuckleball is indeed accompanied by complex flow physics that are hereby clarified in most part, yet without eliminating the unpredictability that makes the pitch a vital part of the game of baseball. The study is also applicable in passive measure of flow control in general.

Acknowledgement

The authors would like to thank Prof. William Saric for fruitful discussion and his insight regarding the interpretation of the present results. The experiment described in this paper was conducted at the Institute of Fluid Science, Tohoku University during the first author's sabbatical leave there. The authors wish to thank Prof. Y. Kohama at the Institute of Fluid Science for making this collaboration between the present authors possible.

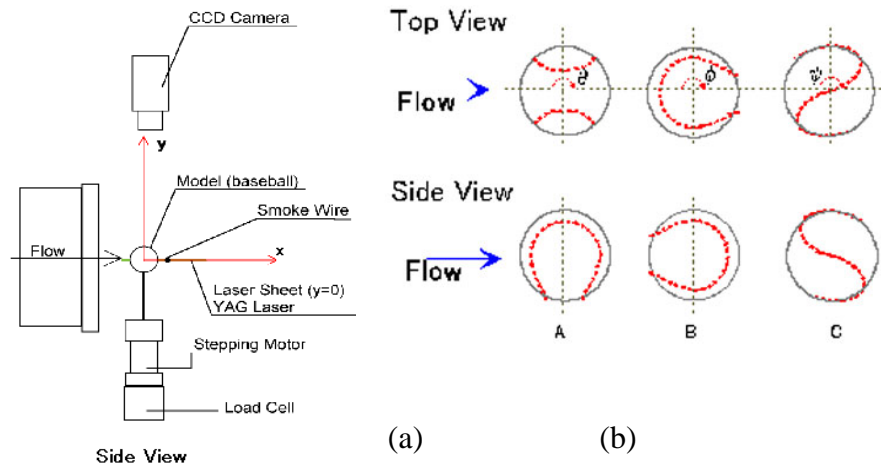
References

- ¹Mehta, R. D., 1985, "Aerodynamics of Sports Balls," Annual Review of Fluid Mechanics, Vol. 17, pp. 151-189.
- ²Anonymous, "Official Rules," Major Baseball League, The Office of the Commissioner of Baseball, New York, NY, www.mlb.com, 2008
- ³Adair, R. K., 1995, "The Physics of Baseball," Physics Today, Vol. 48, pp. 26-31 (see also the book of the same title, HarperCollins, 1995.)
- ⁴Watts, R. G. and Bahill, A.T., "Keep Your Eye on the

- Ball, Curve Balls, Knuckleballs, and Fallacies of Baseball," 2000, W.H. Freeman and Co., NY
- ⁵Briggs, L.J., 1959, "Effect of Spin and Speed on Lateral Deflection (Curve) of a Baseball and Magnus Effect for Smooth Spheres," American Journal of Physics, Vol. 27, pp. 589-596.
- ⁶Mizota, T., Kubo, H., Okajima, A., 1995, "Erratic Behavior of Knuckleball (1) Quasi-Steady Flutter Analysis and Experiment," Journal of Wind Engineering, Vol. 62, pp. 3-14 (in Japanese.)
- ⁷Mizota, T., Kubo, H., Okajima, A., 1995, "Erratic Behavior of Knuckleball (2) Wake Field and Aerodynamic Forces," Journal of Wind Engineering, Vol. 62, pp. 15-22 (in Japanese.)
- ⁸Himeno, R., 2001, "Computational Study of Influences of a Seam Line of a Ball for Baseball on Flows," Journal of Visualization, Vol. 4, No. 2, pp. 197-207.
- ⁹Watts, R.G. Sawyer, E., 1975, Aerodynamics of Knuckleball," American Journal of Physics, Vol. 43, pp. 960-963.
- ¹⁰Kohama, Y., Kobayashi, R. and Ito, H., 1982, "Performance of the Small Low-Turbulence Wind Tunnel," Mem. Inst. High Speed Mech., Tohoku University, Vol. 48, pp. 119-142 (in Japanese).
- ¹¹Ito, H., Kobayashi, R. and Kohama, Y., 1992, "The Low-Turbulence Wind Tunnel at Tohoku University," Aeronautical Journal, Royal Aeronautical Society, pp. 141-151.
- ¹²Sawada, H., Kunimasu, T and Suda, S., Sphere Drag Measurements with the NAL 60cm MSBS," J. of Wind Engineering, No. 98, January 2004, pp. 129-136 (in Japanese.)
- ¹³Higuchi, H., Sawada, H. and Kato, H., "Sting-free Measurements on a Magnetically Supported Right Circular Cylinder aligned with the Free Stream," Journal of Fluid Mechanics, Volume 596, Pages 49-72, February 2008.
- ¹⁴Jeon, S., Choi, J., Jeon, W., Choi, H., and Park, J., "Active Control over a Sphere for Drag Reduction at Subcritical Reynolds Number," Journal of Fluid Mechanics, Vol. 517, 2004, pp. 113-129.
- ¹⁵Bigger, R., Higuchi, H. and Hall, J.W., "Open-Loop Control of Disk Wakes in Air and Water," AIAA Journal Vol.47, No.5, May 2009.
- ¹⁶Schubauer, G. B. and Spangenberg, W.G., 1960 "Forced Mixing in Boundary Layers," Journal of Fluid Mechanics, Vol. 8, Part 1, pp. 10-31.
- ¹⁷Amitay, M., Horvath, M., Michaux, M., and Glezer, A., "Virtual Aerodynamic Shape Modification at Low Angles of Attack using Synthetic Jet Actuators," AIAA Paper 2001-2975, June 2001.
- ¹⁸Achenbach, E., 1972, "Experiments on the Flow past Spheres at Very High Reynolds Numbers," Journal of Fluid Mechanics, Vol. 54, Part 3, pp. 565-575.
- ¹⁹Achenbach, E., 1974, "The Effects of Surface Roughness and Tunnel Blockage on the Flow past Spheres," Journal of Fluid Mechanics, Vol. 65, Part 1, pp. 113-125.

²⁰Sakamoto, H., Haniu, H., 1990, "A Study on Vortex Shedding from Spheres in a Uniform Flow," Journal of Fluids Engineering, Vol. 112, December, pp. 386 -392.

²¹Weaver, R., "Comment on 'Aerodynamics of a Knuckleball'" American Journal of Physics, Vol. 44, No. 12, p. 1215, Dec. 1976.



(a) (b)
FIGURE 1 (a) EXPERIMENTAL SET UP (b)REFERENCE ORIENTATION OF BALL AXIS

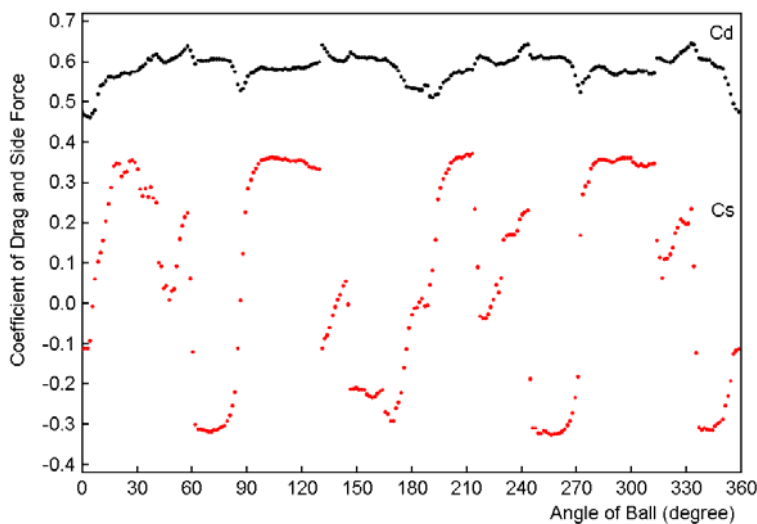
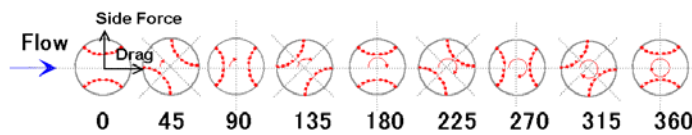


FIGURE 2 DRAG COEFFICIENT AND SLIDE FORCE COEFFICIENT AT VARIOUS BALL ORIENTATION (BALL AXIS A) (TOP VIEW OF THE SEAM PATTERN IS ALSO SHOWN)

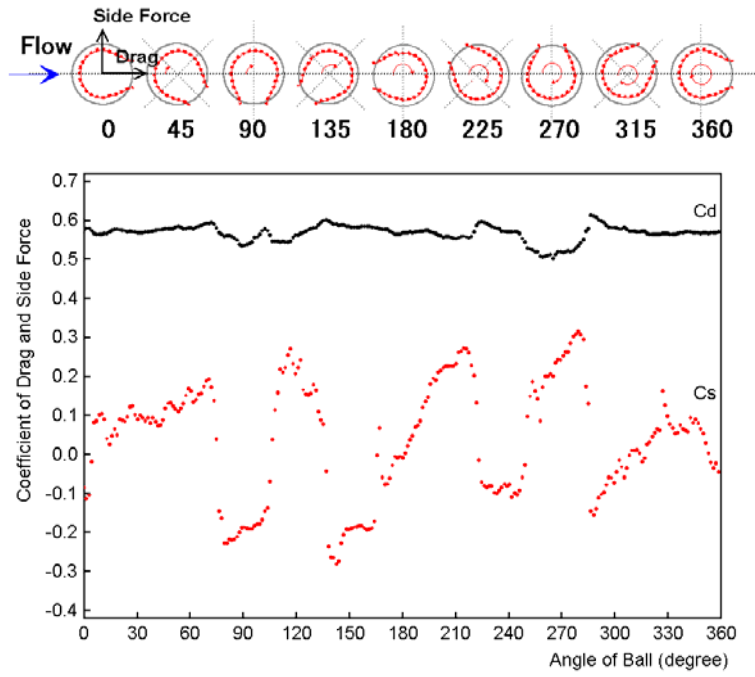


FIGURE 3 DRAG COEFFICIENT AND SLIDE FORCE COEFFICIENT AT VARIOUS BALL ORIENTATION (BALL AXIS B)

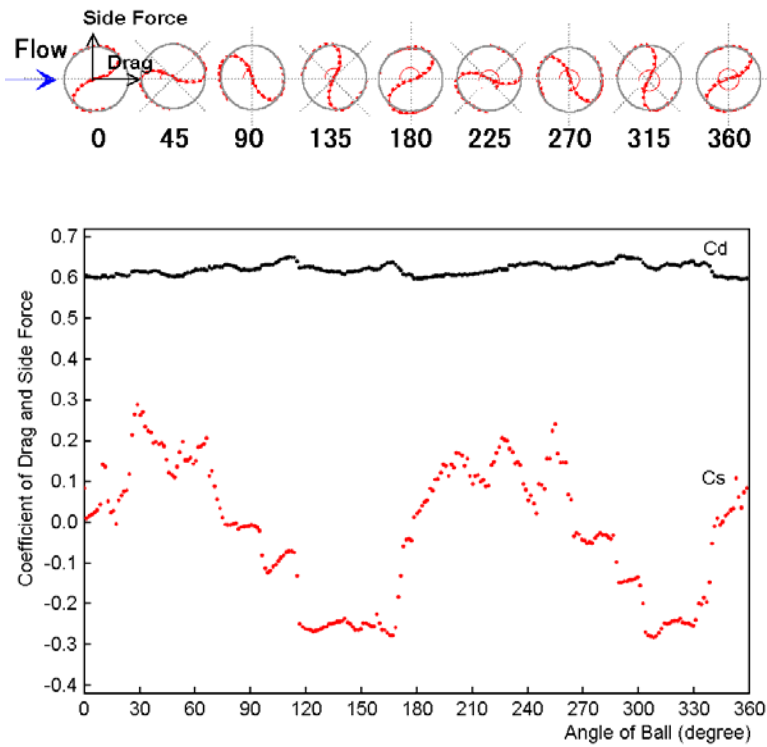


FIGURE 4 DRAG COEFFICIENT AND SLIDE FORCE COEFFICIENT AT VARIOUS BALL ORIENTATION (BALL AXIS C)

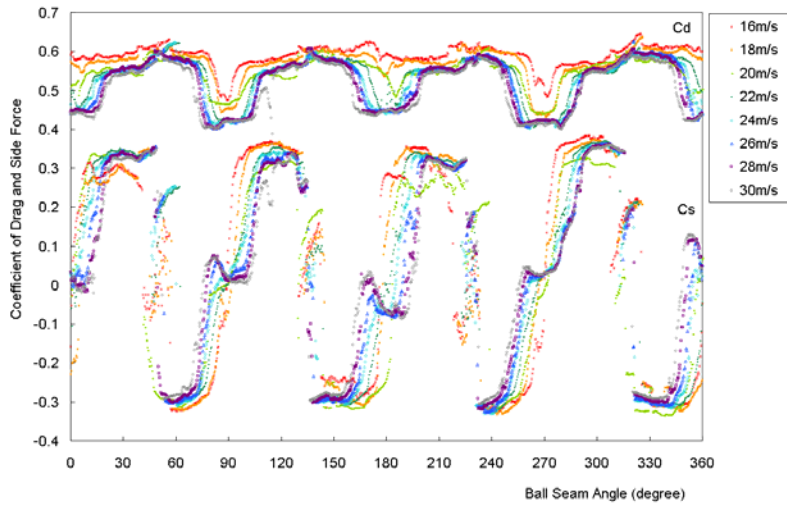


FIGURE 5 DRAG COEFFICIENT AND SIDE FORCE COEFFICIENT AT VARIOUS SPEEDS (BALL AXIS A, REYNOLDS NUMBER RED=0.75E5~1.43E5)

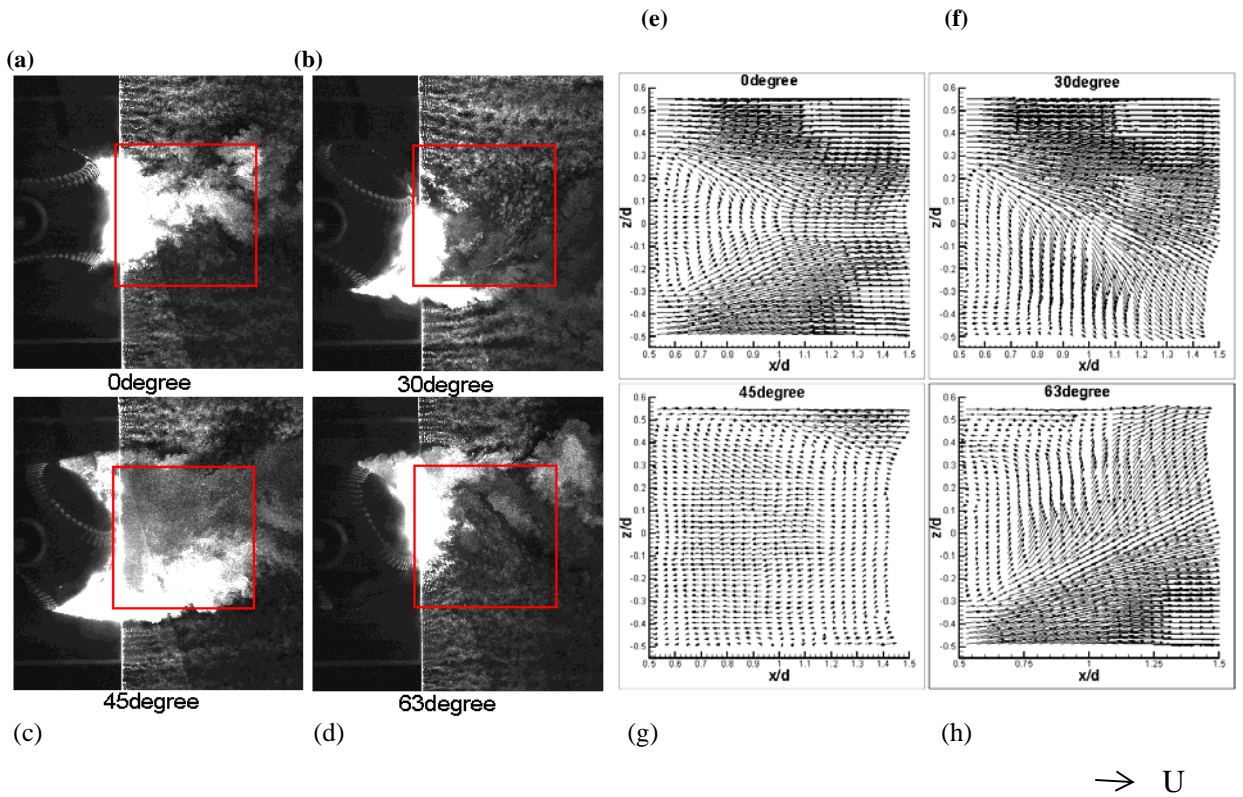


FIGURE 6 SIDE-VIEW FLOW VISUALIZATIONS AND VELOCITY DISTRIBUTIONS IN THE MARKED REGIONS

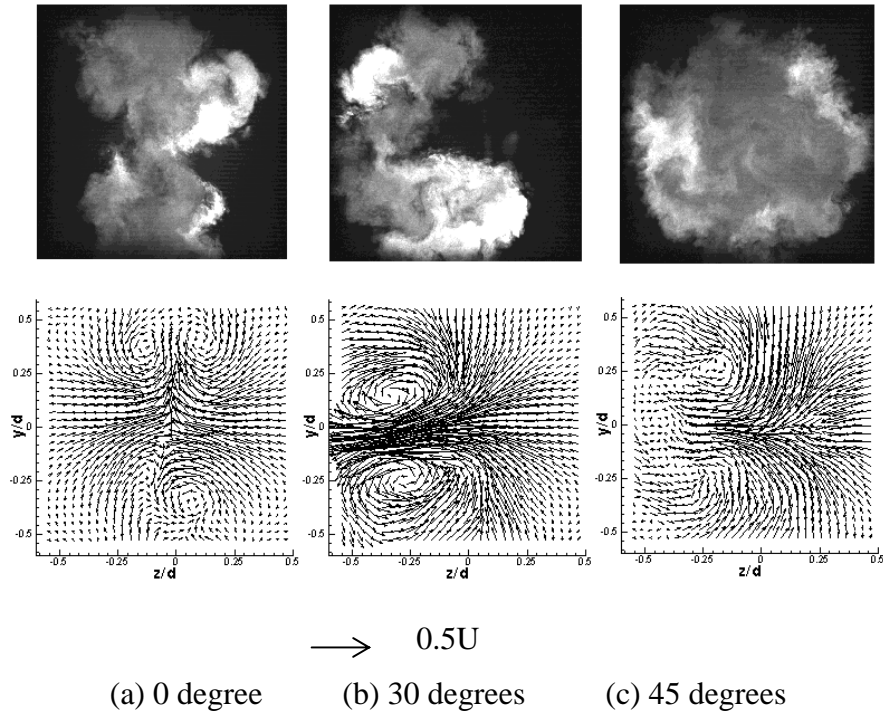
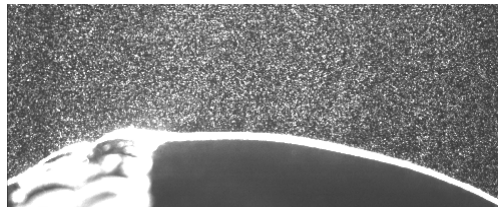


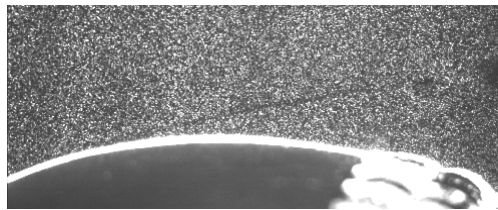
FIGURE 7 END VIEW FLOW VISUALIZATIONS AND VELOCITY FIELDS AT X/D=1.



(a) 30 degrees

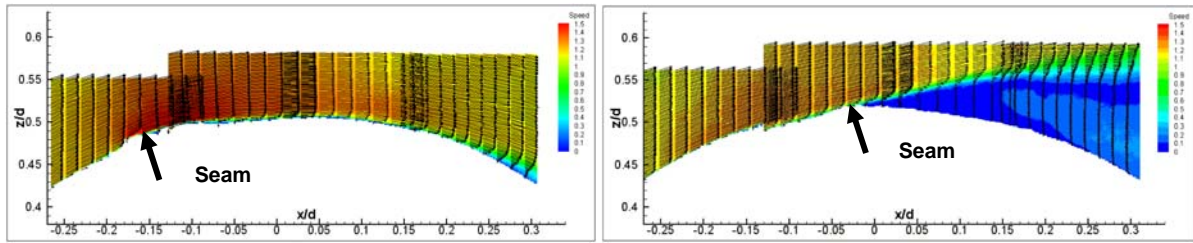


(b) 45 degrees



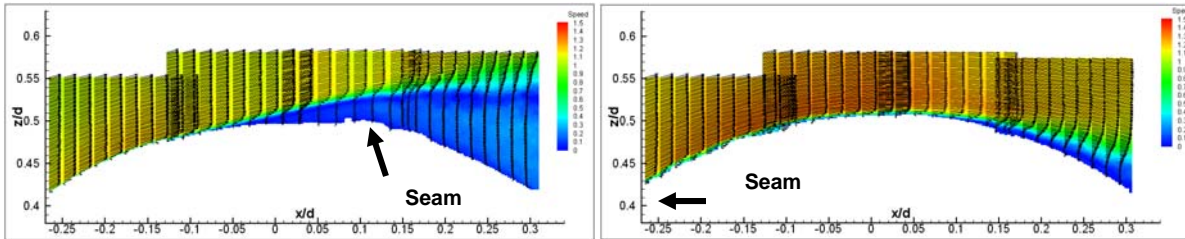
(c) 60 degrees

FIGURE 8 PARTICLE VISUALIZATIONS OF THE FLOW OVER THE SURFACE WITH SEPARATING BOUNDARY LAYER



(a) 30 degrees

(b) 45 degrees

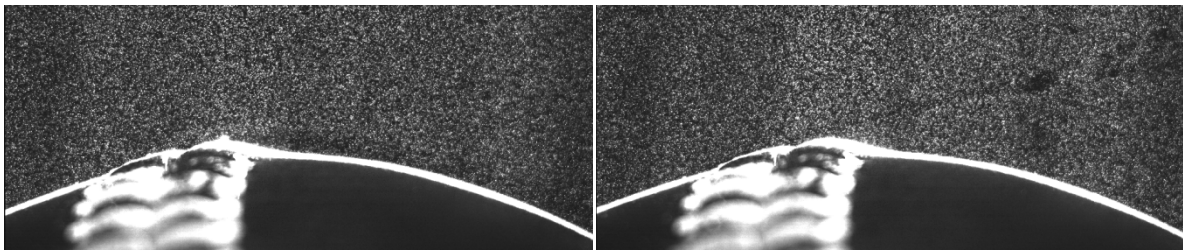


(c) 60degrees

(d) 90degrees

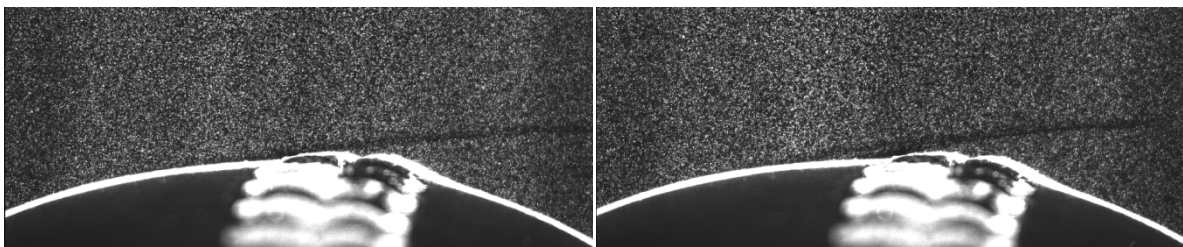
→ U

FIGURE 9 VELOCITY VECTOR FIELD IMMEDIATELY ABOVE THE SURFACE AT DIFFERENT SEAM POSITIONS



(a) 36 degrees

(b) 37 degrees



(c) 50 degrees

(d) 52 degrees

FIGURE 10 EFFECT OF SMALL ANGLE CHANGE ON FLOW.